275 kV cable discharge field measurement and analysis of SVLs chain failure using ATP

F.Ghassemi[a], S.Dennis[a], A.Ainsley[a] A. Manu Haddad[b], S.Robson[b]

[a]*National Grid Electricity Transmission, National Grid House, Warwick Technology Park, Gallows Hill, Warwick EC34 6DA, United Kingdom*
[b]*Cardiff University, Cardiff CF24 3AA, United Kingdom*

Abstract

Results of field measurement of trapped charges on a 275 kV cable will be presented. The instrumentation and calibration method used in the measurement will be discussed. It will be shown that if the cable is not force-discharged by means of earth switches, the trapped charges will decay very slowly. The atmospheric parameters such as humidity and temperature affect the discharge time, which also depends on how much of the circuit is exposed to open air.

The measurement results are used in EMTP-ATP simulation to confirm that trapped charges may be sufficient to cause sheath voltage limiters (SVL) of the cable to fail. The number of SVL breakdown depends on the mode of SVL failure, i.e. whether it attains low impedance (short circuit) or open circuit when the energy absorbed exceeds the rating.

1. Background

The phenomena of cable charging and discharging have been a concern to cable engineers especially when performing commissioning tests and during maintenance work [1,2]. Also, the charging/discharging phenomena have received special attention from utilities which are using high-voltage (HV) cables for voltage control during periods of light load which requires nightly switching of cables. For this particular activity, the earth switches of the cable are not usually used due to excessive wear and tear of switch contacts and also, in accordance with their internal recommendations for safety and security of supply, some utilities require that earth switches can only be operated if relevant staff is present in the substation.

A study was carried out to investigate the root cause of excessive SVL failures in a number of EHV cables. The EMTP programme was used to model a cable circuit with high SVL failure rate. The cable design detail is given in Appendix A. The results of the study were presented in IPST 2013 [3]. The study showed that if sufficient trapped charges remain on the isolated cable long enough, i.e. until the next switching action some six to eight hours later, then there is a very high probability that the overvoltage surges on the core and thus sheath were sufficient enough to cause SVL failure. It was shown that this was the only condition that would lead to failure and that the SVL would have had adequate energy absorption capability for other transients on the cable such as energisation with no trapped charges, lightning on the relevant overhead lines connected to the cable and external faults, all of which had been considered during the design stage.

It is usually assumed that the trapped charges on an isolated cable are drained to earth within a short time of a few hours through the cable insulation losses. Very few test results of cable charging and discharging can be found in the literature [4]. No guideline is provided by IEC or CIGRE on the discharge time of extra high-voltage (EHV) single phase cables. For this reason, National Grid, UK, performed a series of cable discharge tests on a 275 kV pressurized-oil-filled (POF) cable of 21 km length, to examine the discharge time of the cable after being isolated and the effect of trapped charges on the sheath voltage limiters (SVL) failure [3,5]. Ref. [6] investigated the effect of cable faults on SVL failure.

This paper describes the method of instrumentation used for measuring dc charges on the cable and estimates the discharge time constant. Field mill devices were used to carry out non-intrusive tests. The paper presents the results of calibration tests in the laboratory that were necessary to confirm the linearity of the transfer ratio of the probe for measuring the system voltage (50 Hz) and the voltage due to trapped charges (a decaying dc signal) when the measurement probes are placed in the field.

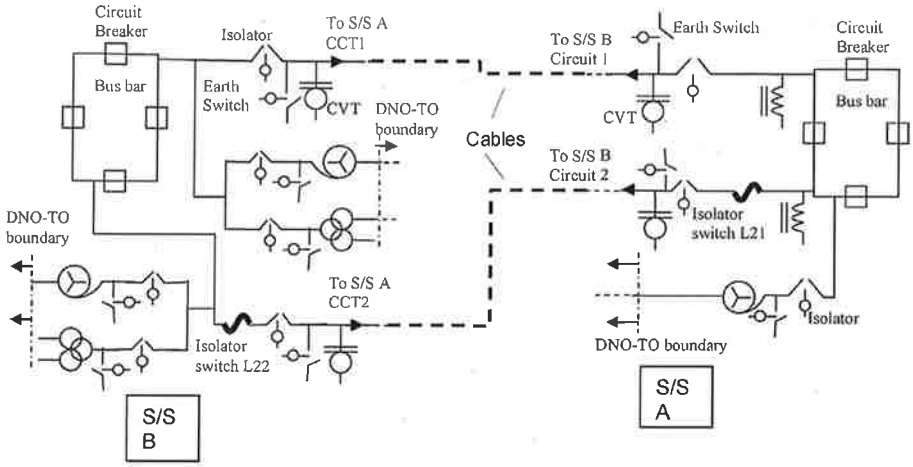

Fig. 1. High level substation A and B layout.

2. The cable under study

The cable circuit considered in the study consists of two parallel, three-phase, 275 kV, 1600 mm^2, copper conductor, oil-filled paper insulated cables. Each circuit consists of three single phase cables. They connect substations (S/S) A and B. The cable detail is given in Ref. [3], which also illustrates the crossbonding used in the cable installation considered in the study. The cores are transposed at every junction, which leads to more balanced impedances in all three phases. The sheaths are cross-bonded as shown in Ref. [3].

Fig. 1, illustrates the high-level layout at S/S A and B. Circuit 2 is used nightly for voltage control by switching it out of service during the night usually between 22:00 and 7:00 the next day. The switching is done remotely from the National Control Centre. Although both circuits have earth switches at both ends, they are only operated when the cables are taken out of service for a long period of time, e.g. maintenance. For regular voltage control switching, these switches are not operated because (i) they can only be operated locally at the substations for safety issues, and (ii) to avoid excessive wear and tear of isolator switches contacts. Both S/S A and B are unmanned.

The cables lengths for Circuit 1 and Circuit 2 are respectively 21.22 km and 21.74 km. The cables are placed in trenches along the route with an average depth of 1 m. They enter tunnels in the vicinity of substations for a short distance. The cable sealing ends at ground level are connected to a piece of overhead horizontal busbar with a length of about 13.5 m as depicted in Fig. 2. The busbar is supported by two vertical insulator poles, each with a vertical axial length (not creepage) of approximately 2.4 m. The isolator switches L21 and L22 are situated at the end of the busbar sections.

As can be seen from Fig. 1, the voltage transducers at both ends of the cables (not shown in Fig. 2) are of capacitive voltage transformer

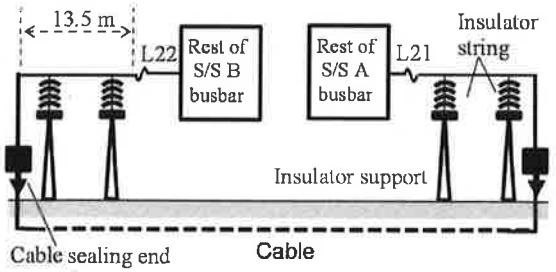

Fig. 2. Cable connection to the air busbar.

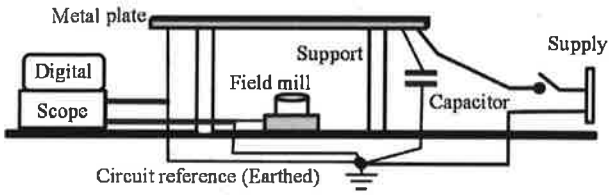

Fig. 3. Field mill test setup.

type with no dc transfer capability. This means that the trapped charges can only drain through the cable insulation losses and stray resistance of the outdoor insulation string at both ends.

3. Measurement method

A non-intrusive measurement system was devised. The main component of measurement system was the field mill. These devices give an out voltage in proportion to the electric field that is imposed on them [7].

A series of tests were carried out to examine the relationship between the input, i.e. electrostatic field and the field mill output voltage. This was essential to ensure that the field mill has a constant transfer ratio between input and output signals for both dc and ac signals which, in turn, allows the field mill to be calibrated in the field when it is installed under the live busbar for 50 Hz voltage and measuring correctly when the cable is switched out of service with trapped charges, e.g. dc voltage on the cable.

A metal plate was used as a source for electric field. In order to increase the capacitance of the plate with respect to earth a 12 μF capacitor was connected to the plate, which was then energised to the mains voltage of 220 V, 50 Hz. The neutral of the mains was earthed. The metal plate was raised from the surface to a height of 0.7 m by using non-metallic supports. The field mill was placed under the plate. Fig. 3 shows the test set up. The voltage of the metal plate was measured directly by Channel 1 of a digital oscilloscope and the output of the field mill was measured by Channel 2. The plate and the connected capacitor were energised by closing the switch. After waiting for a few minutes, the voltage was removed. The capacitor was then discharged through the input resistance of the oscilloscope of 10 mΩ. The capacitor losses also contribute to the discharge time constant.

Figs. 4 and 5 show the plate/capacitor voltage measured directly by the oscilloscope and by the field mill respectively for disconnection at nearly zero and peak of the source voltage. As expected,

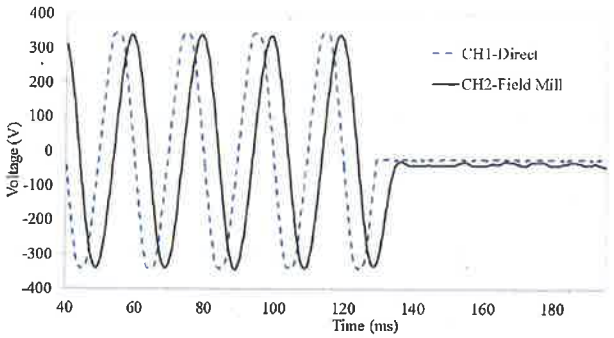

Fig. 4. Test rig calibration, switching off at nearly zero voltage.

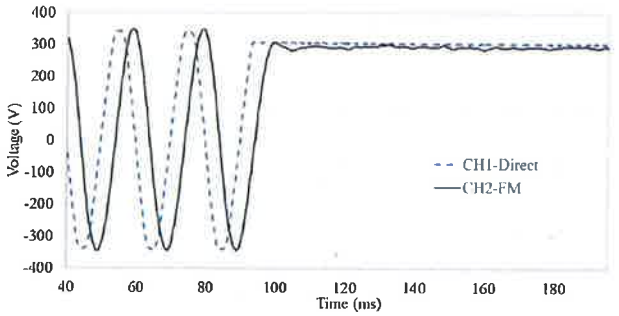

Fig. 5. Test rig calibration, switching off at nearly peak voltage.

there is a 90° phase shift between the direct measurement, i.e. the voltage of the plate and the measurement by the field mill which is proportional to the electric field. It can also be deduced that the transformation ratio between the input and output of the field mill is constant for the ac part of the signal, i.e. when the plate is connected to the mains, and after the voltage is removed, the plate voltage discharges very slowly. Thus, it was confirmed that the field mill can be calibrated using the 50 Hz voltage by placing it under the live busbar. When the voltage is removed, the field mill correctly measures the dc voltage on the cable connected to the exposed busbar.

4. Field measurement

The objective of the measurements in 2015 and 2016 was to monitor the slow changing dc voltage on the core of the cable, hence, the frequency response of the field mill probe was not critical. The device's output is an analogue voltage that was then fed onto an analogue-to-digital converter with a sampling rate of one second and storage capability for longer than four weeks. The data was later downloaded to a permanent storage. Note that since the sampling rate of the recorder is 1 s, the 50 Hz signal is not sampled accurately. However, measurement of 50 Hz signals or transients associated with switching were not part of the scope of the measurement. Thus, a low pass filter was used on the sampled data to reduce the noise due to aliasing.

The field mills, one for each phase were placed under the section of the busbar between the first insulator string nearest to the cable sealing end and the second insulation string closest to the switch, see Fig. 2. The vertical distance between the field mill and the busbar was approximately 3 m. The atmospheric parameters namely, temperature, relative humidity and pressure (THP) were also recorded at both S/S A and B close to the air busbar where the field mills were placed. The recording was performed at the sampling rate of 30 s. Recording of THP was essential to verify the dependency of the discharge through exposed part of the circuit,

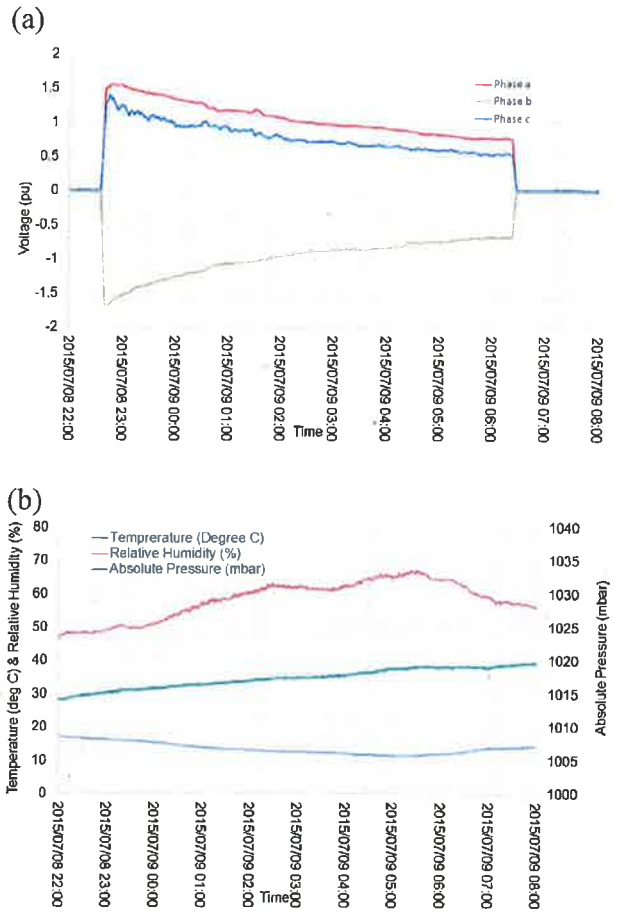

Fig. 6. (a) Measured trapped charge voltages on the three phase system on 8/7/2015. (b) Measured THP measured on 8/7/2015.

e.g. insulator strings, to the atmospheric parameters, whose effect on the insulation losses of a trenched cable is very low.

Fig. 6a illustrates the measured voltages on the three-phase system, and Fig. 6b shows the measured temperature, relative humidity and pressure (THP) for a day in the second week of July 2015. The highest voltage at the time of switch off reached 1.7 per unit (pu) with respect to the peak of the nominal phase voltage ($275\frac{\sqrt{2}}{\sqrt{3}} = 224.5$ kV) which decayed to about 0.75 pu at the time of cable re-energisation. Higher than nominal voltages at the time of de-energisation can be expected in cables and capacitive switchings due to restrike in circuit breakers. The maximum and minimum temperatures during the measurement period were about 17 and 11 °C respectively with the relative humidity remaining below 70%.

Logarithmic linearization was used to determine the discharge time constants. The decay time constant is defined as the time for an exponentially decaying curve to reduce from its peak to 1/e or 37% of the peak. Fig. 7, illustrates the rate of change of voltage as the linear lines at different times during discharge. Two distinct time constants can be identified, one is when the cable was switched out for about two hours when the time constant is about 6 h increasing to about 13 h at around the time of the cable re-energisation. It can be seen from the record that the temperature was in fact increasing and humidity reducing, leading to increase in the time constant.

Fig. 8a and b illustrates the measured trapped charge voltages and atmospheric parameters records during another period starting 21/7/2015. The same effects can be observed. It can be seen from Fig. 8a that the slowdown in the discharge is clearly visible at

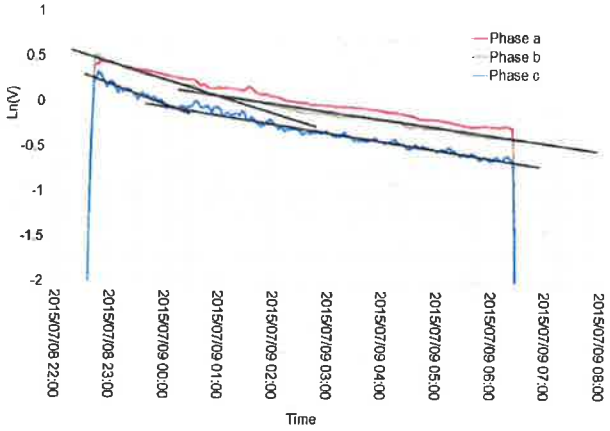

Fig. 7. Determination of rate of change of voltage for 8/7/2015.

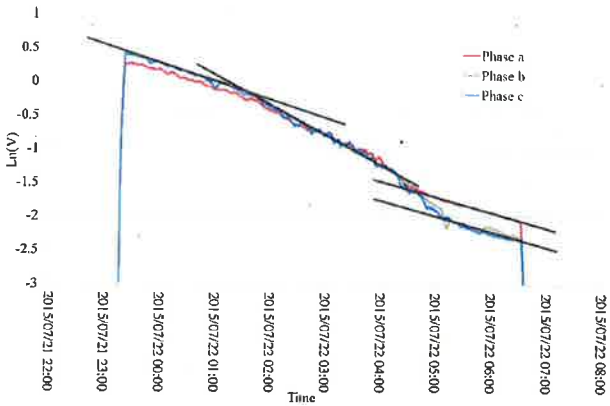

Fig. 9. Determination of rate of change of voltage for 21/7/2015.

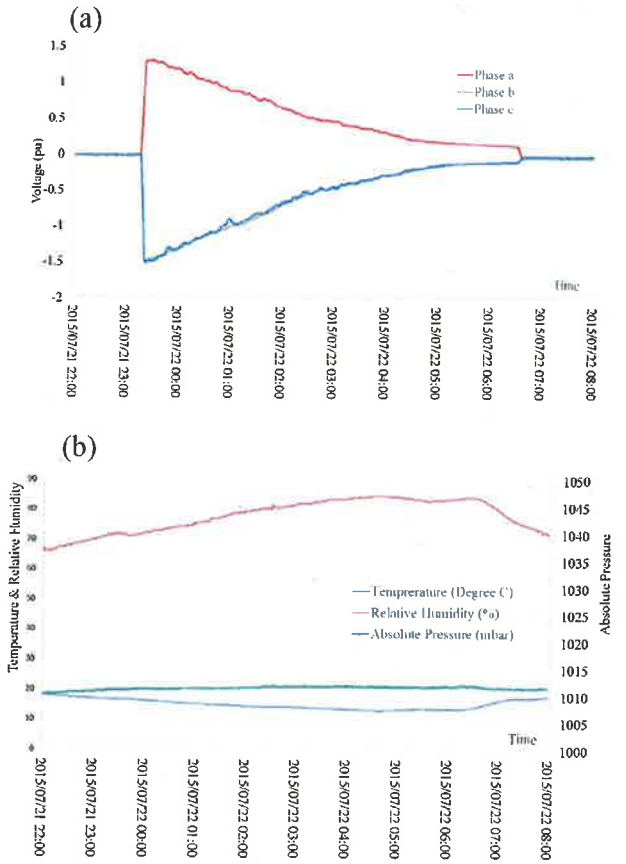

Fig. 8. (a) Measured trapped charge voltages on the three phase system on 21/7/2015. (b) Measured THP for 21/7/2015.

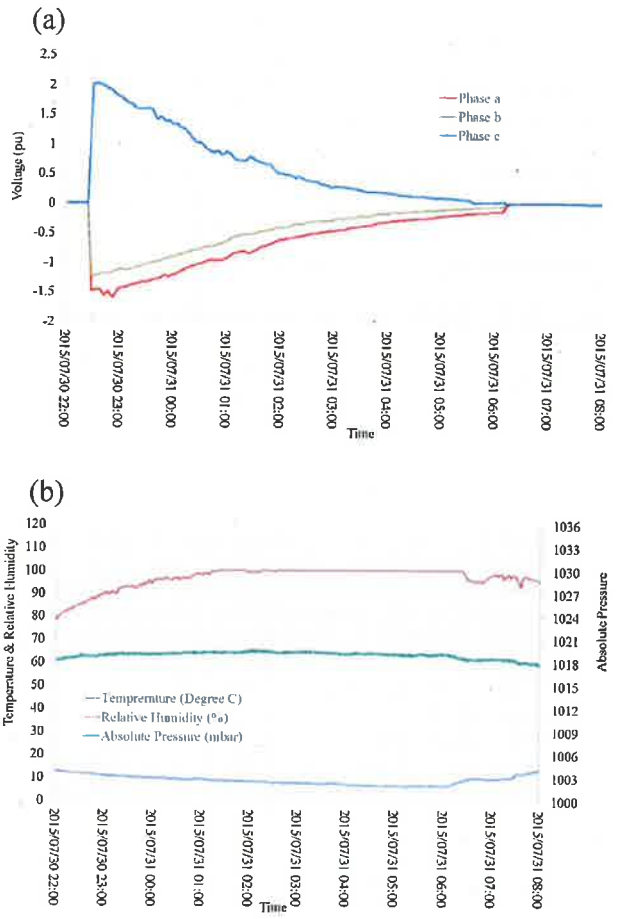

Fig. 10. (a) Measured trapped charge voltages on the three phase system on 30/7/2015. (b) Measured THP on 30/7/2015.

around the time when the cable is about to be re-energised. This correlates very well with the temperature and humidity when the former increased and stabilised and the latter reduced markedly at around the same time. This is very clearly visible in Fig. 9, that shows the rate of change of discharge when it changed at the same time as changes in temperature and humidity. At the time of re-energisation, about 13% voltage was still on the red phase of the cable which fell from about 128% of voltage at the time of disconnection.

Fig. 10a, illustrates the voltages for a de-energisation in 30/7/2015. It can be seen that the voltages reached nearly 2 pu and decayed to a very low level by the time the cable was re-energised. Fig. 10b shows the change in atmospheric parameters. It can be observed that the relative humidity was very high reaching 100% while the temperature dropped to as low as 6 °C. The duration of high humidity was relatively long. Two distinct time constants can be observed, first was about 3.5 h changing to shorter time constant of about 1.5 h. The cable is virtually discharged in about 5 h (Fig. 11).

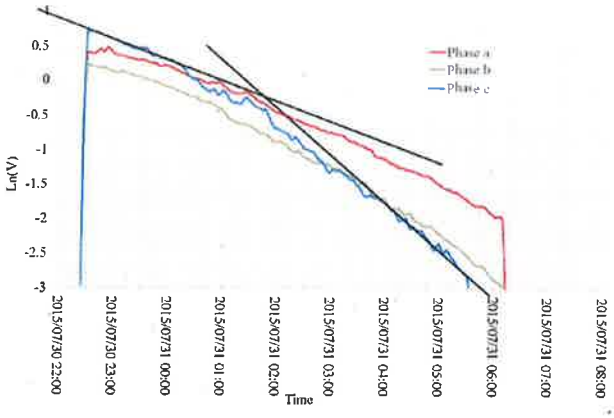

Fig. 11. Determination of rate of change of voltage for 30/7/2015.

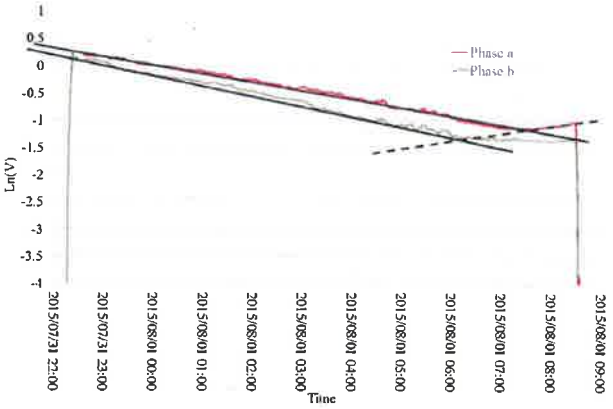

Fig. 13. Rate of change of voltage for 31/7/2015.

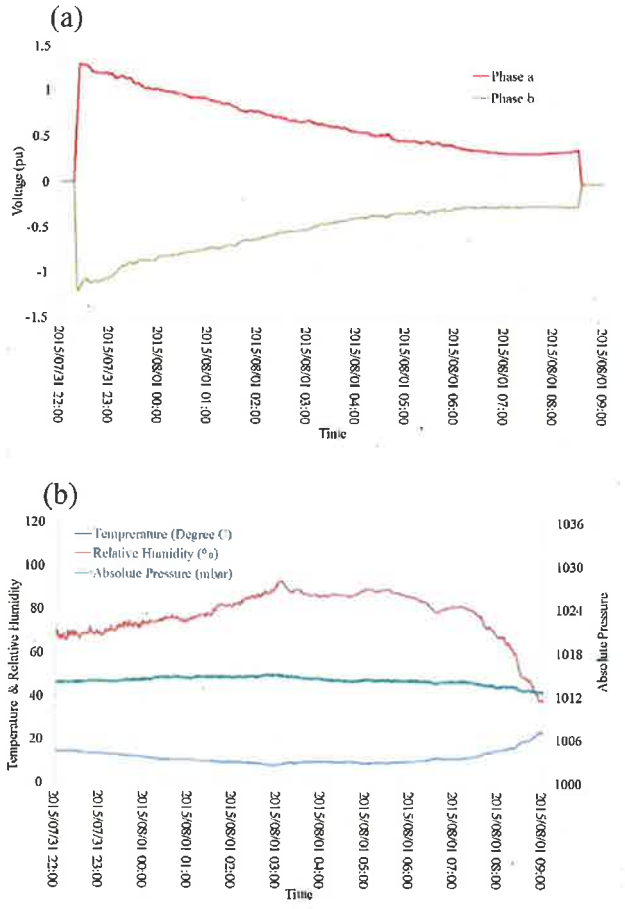

Fig. 12. (a) Measured trapped charge voltages on three phase system on 31/7/2015. (b) Measured THP on 31/7/2015. (For interpretation of the references to colour in the text, the reader is referred to the web version of this article.)

Fig. 12a, illustrates the voltages on the red and yellow phases. The blue phase measurement is missing. This was due to flat battery in the field mill and associated recorder, which was detected after measurement was completed. It can be seen that the voltage on the red phase reaches 1.3 pu at the time of de-energisation, falling to about 0.3 pu the next day at around 7 am when it starts to increase again. The temperature was not particularly low and it started to increase at around 4 am on 1/8/2015 reaching 18 °C at the time of the switching. Likewise, the humidity fell sharply in the morning. Fig. 13 shows the rate of change of voltage on the cable. The positive rate of change of voltage just before energisation is shown by the broken straight line. The increase in the phase voltages can be attributed to the coupling with the live adjacent busbar and increase in the system loading which, in turn, induces higher voltage in the cable. This increase offsets the discharge of the cable through the insulator strings.

Therefore, depending on the substation layout, the disconnected cable may in fact be charged up due to induction, if it is not earthed.

Ref. [5] provides details for estimating the time constant of discharge of a cable when it is not earthed. The atmospheric parameters variations should be taken into account when there is an exposed part of the cable circuit. Note also that the rate of discharge is also a function of the initial voltage and temperature of the cable (core/insulation) [5]. As can be seen from all the records shown in this paper, the initial rate of change of voltage on the cable changes within a couple of hours after de-energisation. This is influenced not only by the atmospheric parameters but also by the voltage magnitude on the core.

5. Maintenance records

The cable has 18 junction boxes, of which 14 contain SVLs, hence, a total of 42 SVLs limit the sheath voltage. Which phase SVL fails most appear to be random but, usually, at least two phases SVLs fail in each junction box. Almost always, the SVLs close to the substation fail when switching is performed.

Two maintenance reports will be presented in this section. The objective is to check whether any correlation between atmospheric parameters and SVL failures exists.

In March 2011, there was fire in one of the junction boxes. All three SVLs in the junction box had catastrophically failed (destroyed). The subsequent check on earthing and connections in the junction box showed that all connections were according to the guidelines. The SVLs were changed and the cable was put back in service. Thermovision tests showed that no hotspot existed in the junction box and all connections, including earthing, were satisfactory.

The weather record for spring 2011 revealed that March 2011 was exceptionally warm and dry month. It was one of the warmest on record with much below average rainfall (http://www.metoffice.gov.uk/climate/uk/interesting#y2011).

On 18/06/2015, the cable was de-energised for routine maintenance. Six SVLs on the route had to be changed. The test to assess the SVL condition involves applying a test voltage and measuring the leakage current. If the current exceeds the declared value by the

manufacturer, the SVL is discarded. At this point of time all SVLs were healthy.

The cable was put back in service and then taken out on 18/7/2015. In total, 13 SVLs were found to have failed. Note that network loading reduces to a minimum of about 36% of the maximum load in winter. Therefore, the cable was used more regularly for voltage control. Inspection of the weather records revealed that June/July of 2015 were one of the hottest periods on record. The temperature on 1/7/2015 set a new record (http://www.metoffice.gov.uk/climate/uk/interesting#y2015).

The maintenance and SVL failure records correlate very well with the weather condition and findings of this paper.

6. EMTP-ATP simulation

Ref. [8] shows that if the trapped charges observed on 8/7/2015, shown in Fig. 6a, were considered in the model, two SVLs in the first junction box would fail. Note that the other trapped charge levels at the time of cable energisation, measured and presented in this paper, were not high enough to cause any SVL failure.

The same model described in Refs. [3] and [8] is used here to examine the chain failure of SVLs at different junction boxes. Note that Ref. [8] assumed that, at the time a SVL's absorbed energy exceeds its rating of 31 kJ, the SVL impedance reduces to zero and it becomes like a short circuit. It was also shown that the secondary transient generated by the collapse of voltage at the terminal of the first failed SVL was responsible for the breakdown of the adjacent SVL on the other phase in the same junction box [8]. The purpose of this section is to examine whether the SVLs in other junction boxes would also breakdown when the failed SVLs are no longer operating correctly. The model used to represent the SVL is shown in Appendix B. The earthing impedance of the junction boxes is assumed to be 15 Ω for all results presented hereafter [3,5,8].

For all the tests that follow, the trapped charges at the instant of cable energisation are considered to be 0.75, −0.75 and 0.55 pu of the peak of the nominal voltage in phases a, b and c respectively. The energisation is assumed to occur at the positive peak of the nominal voltage on Phase b.

First, it is assumed that the failed SVLs change their impedance to a short circuit when they fail. In the model, it is replaced with a short-circuit at the instance of the SVL failure. The currents in and voltage across the SVLs in Junction Box JB2174 are shown in Fig. 14(a). The Y-axis is in kV for voltages and kA for currents. As can be seen, the voltages in Phases a and b clip at around 21 kV and −21 kV respectively, which are in line with the expected levels in the SVL datasheet. The corresponding initial currents in the SVLs are around 14 kA. The energy absorbed by the SVLs in the first junction box, JB2174, located 1.547 km away from the closing circuit breaker is shown in Fig. 14(b). As can be seen, Phases b and a are the first and second SVLs to fail. The SVL on Phase a fails as a result of the secondary transient produced by the Phase b SVL breakdown [8]. No other SVL fails.

The same amount of trapped charges are now considered but with the failed SVLs, in Phase b and Phase a in JB2174 replaced with very low resistance element (0.001 Ω) to represent short circuited SVL. All other parameters in the model remain the same. Fig. 15 illustrates the energy absorbed by the SVLs in the next junction box, JB2167. As can be seen, the SVLs in Phases a and b have failed in a much shorter time. This may be attributed to the fact that the opposite polarity waves on Phases a and b drive much larger current in the loop between junction boxes JB2174, JB2160 and JB2167 when the SVL in the former are replaced with a short circuit representation. This high current and the clipped voltages of 20 kV across the SVLs in Phases a and b in JB2167 with opposite polarity cause high current to flow in the loop limited mostly by the

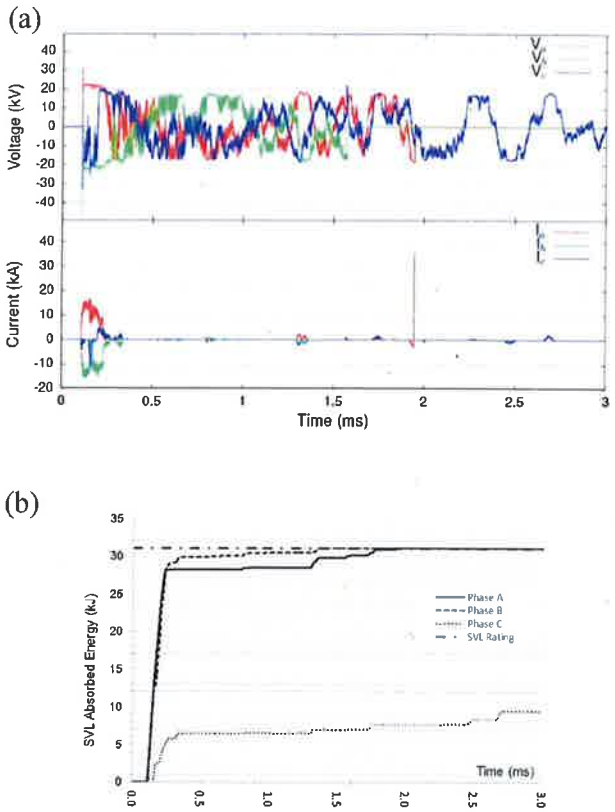

Fig. 14. (a) Computed voltage and current in SVLs at junction box JB2174. (b) Calculated absorbed energy by SVL in JB2174.

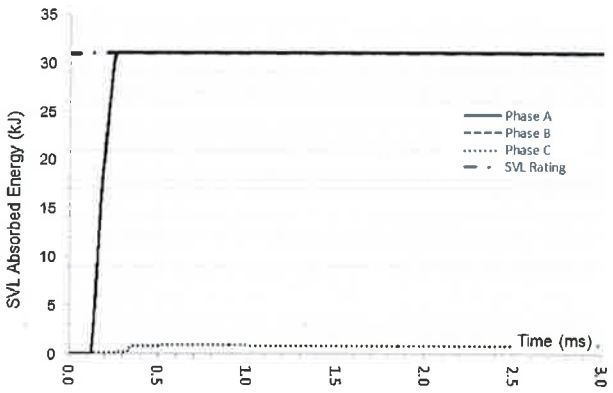

Fig. 15. Calculated absorbed energy by SVL in JB2167.

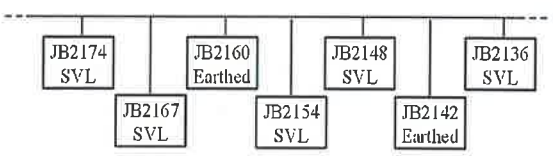

Fig. 16. Junction box locations.

sheath impedance between the junction boxes and the non-linear resistance of SVLs. Note that the junction box on the other side of JB2167 (JB2160), as shown in Fig. 16, is a major point and, therefore, has a physical short circuit to earth, thus making Phases a and b in JB2167 appear between two earthed points with a relatively short distance.

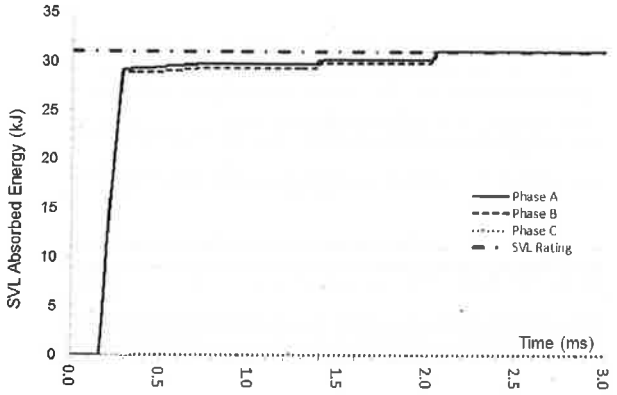

Fig. 17. Calculated absorbed energy by SVL in JB2148.

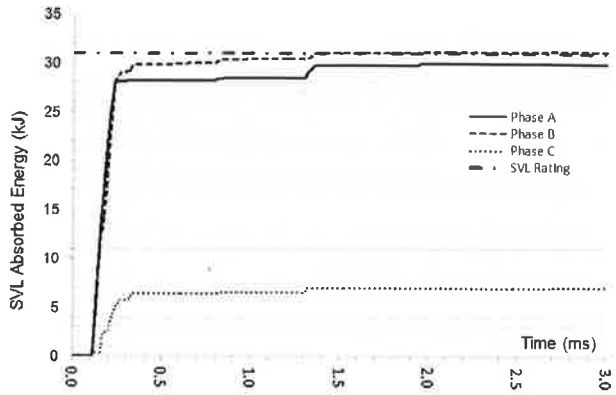

Fig. 18. Calculated absorbed energy by SVL in JB2174 with linear resistance-inductance representing the failed SVL.

If the failed SVLs in JB2167 are replaced with the short circuit and a study is run with all other parameters including the trapped charges configured as before, the SVLs in the next junction box, JB2154, also fail, but after a longer time following switch closing.

The next pair of SVLs to fail is that in junction box JB2148, some 8 km away from the closing circuit breaker. Fig. 17 shows the energy absorbed by the SVLs in junction box JB2148. Note that the SVLs in JB2154 had been replaced with short circuit. These are the last SVLs to fail because the next simulation, with the failed SVLs in JB2148 replaced with very small resistances, showed that the energy absorbed by the SVLs in JB2136 did not exceed the rating.

The above results show that the failure of the first SVL may lead to a chain of failures if the trapped charges are high enough and the SVLs impedances become very low (short circuit mode) after it breaks down. With the first two SVLs in junction box JB2174 failed, the SVLs in JB2167 will also fail with trapped charges at 60%, −60% and 45% of the nominal voltage respectively in Phases a, b and c which would not happen if the SVLs in JB2174 were intact, i.e. healthy.

If it is assumed that the SVLs fail with a short circuit resistance of 0.01 Ω instead of 0.001 Ω, then the SVL in JB2154 in Phase B is the last SVL to fail. If this SVL is replaced with a resistor of 0.01 Ω, then no other SVL will fail, indicating that the low impedance path created by failed SVLs reduces the transient voltages in the sheath. This test shows that the failure mode of SVL and the impedance they adopt when they fail is important in the subsequent SVL failure.

The actual failure mechanism of MOV-based SVLs is not clearly understood. The maintenance team, who test every failed SVL offline, advised that all SVLs exhibit low resistance after failure. However, it is not known what value of resistance exactly a failed SVL adopts under voltage stress in the field.

Using the model, tests were conducted to examine the chain failure mechanism considering two levels of resistance for SVLs after they failed. First, it was assumed that the SVL's non-linear characteristic changes to a linear 100 Ω resistance in series with a 1 μH inductance at the instant its energy exceeds the declared rating of 31 kJ. Fig. 18 illustrates the energy absorbed by the SVLs in JB2174, the nearest junction box to the closing circuit breaker. The model is similar to that used to obtain the results shown in Fig. 14, except for the failure model. As can be seen, only the SVL in Phase b has failed, and the transient generated by the failure is not high enough to cause breakdown of the SVL in Phase a. Replacing the failed SVL in Phase b of JB2174 with linear R–L elements with the above values, the cable was energised again with all parameters including the trapped charges which were kept at the same levels. No other SVL in JB2174 failed. In the next junction box, JB2167, the Phase a SVL failed. Fig. 19 shows the energy absorbed by the SVLs in JB2167. No

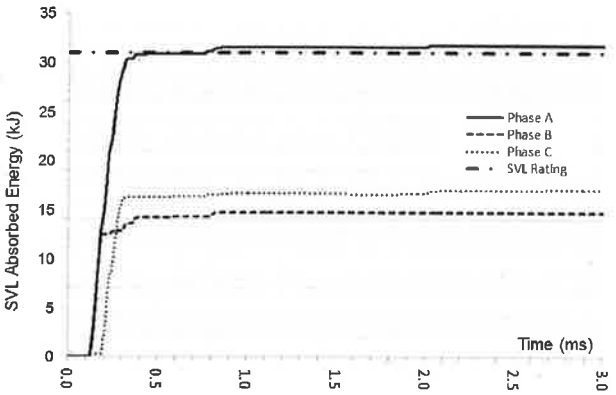

Fig. 19. Calculated absorbed energy by SVL in JB2167 with linear resistance-inductance representing the failed SVL.

other SVLs failed after the faulty SVLs in JB2174 and JB2167 were replaced with linear R–L circuit to represent failure.

Further simulations showed that if SVL breakdown leads to complete open circuit in the SVL, then only one SVL in JB2174 and subsequently one in JB2167 respectively in Phase b and a would fail, for the same levels of trapped charge. In this scenario, SVL failure causes an open circuit in the SVL and then, for subsequent energisation, the failed SVL was replaced by an open circuit. This is similar to the condition with a 100 Ω linear resistor in series with 1 μH inductance to represent the breakdown in SVLs.

7. Conclusions

Field measurement results were presented to confirm that, if a cable is not connected to earth after isolation, for example by means of earth switches, a charge can remain on the cable for a long period of time. Furthermore, it was shown that the rate of decay of the trapped charge is influenced by the atmospheric parameters such as humidity and temperature and the length of the exposed part of the circuit.

SVL failure data was presented together with the weather information during two periods of time when a large number of SVLs had failed. Good correlation was observed between the failure rate and warm/dry weather, confirming that enough trapped charges may remain on the cable until the next energisation and that they were the root cause of the high number of SVL failures.

Using the voltage of trapped charges obtained from measurements at the instant of cable energisation, it was shown through simulation that the mode of SVL failure influences the chain break-

down of SVLs for subsequent energisations. The worst mode is when a SVL's relatively high impedance changes to a short circuit when it fails. It was shown that SVLs up 8 km away may be affected. If, however, it is assumed that a failed SVL becomes open circuit at the instant of breakdown, then the subsequent failures will be less and only SVLs located within shorter distances from the closing circuit breaker are affected, for the same amount of trapped charges.

Appendix A.

The cable is of 275 kV, 1600 mm^2, copper conductor, oil-filled and paper insulated. The cable layout and spacing is shown in Fig. A1. The cable data is given in Table A1. The relative permittivity of the insulation around the sheath is considered to reduce from 8 at 50 Hz to 4.5 at 5 kHz. The overall cable radius is 5.156 cm. The earth resistivity is considered to be 20 Ω m throughout.

The cable joint assemblies are connected to the crossbonding or solid earth link boxes by concentric bonding leads. These are about 7.5 cm apart with lengths of 10 m for all link boxes. The concentric cable data is given in Table A2. The overall radius is 2.46 cm.

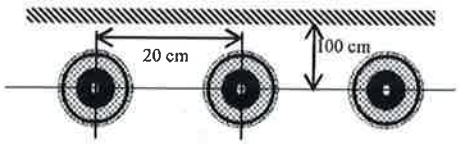

Fig. A1. Cable layout, spacing and trench depth.

Table A1
Cable data.

	Inner radius (cm)	Outer radius (cm)	ρ (Ω m)	μ_{core}	$\mu_{insulation}$	ε_r
Core	0.68	2.675	1.724×10^{-8}	1	1	3.8
Sheath	4.3	4.72	2.13×10^{-7}	1	1	8

Table A2
Concentric cable data.

	Inner radius (cm)	Outer radius (cm)	ρ (Ω m)	μ_{core}	$\mu_{insulation}$	ε_r
Core	0	1.25	1.724×10^{-8}	1	1	3.5
Sheath	1.75	2.16	2.826×10^{-8}	1	1	3

Appendix B.

Fig. B1 shows the model used in the ATP. The voltage across and current through the SVL are sampled. A shunt with a value of 0.1 mΩ is used to measure current. The voltage and current are then multiplied and integrated to estimate the energy absorbed by

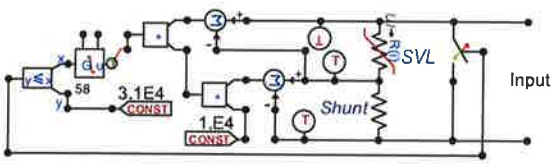

Fig. B1. The SVL model.

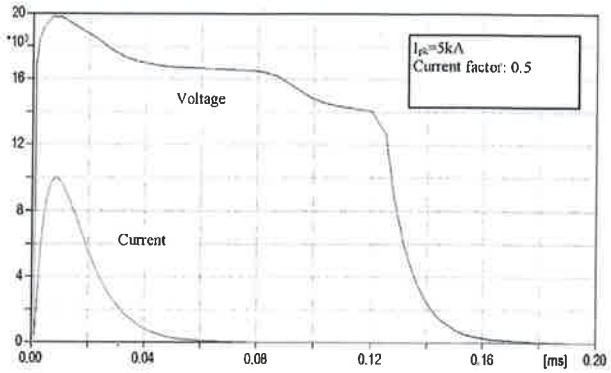

Fig. B2. SVL90 characteristic for 5 kA, 8/20 impulse.

the SVL. This is then compared with the SVL rating of 31 kJ which if exceeded closes the switch across the SVL in the model. The figure shows a case when the SVL changes to a pure short circuit. In cases when finite resistances were considered for the SVL after failure, then a resistor was added in series with the switch.

The SVLs are of SVL90 type. Its V–I characteristic is shown in Table B1. The energy rating is 31 kJ.

Type NLINRES in ATP is used to model the SVL. Several benchmarking of the V–I characteristic is carried out for 8/20 μs impulse wave for different impulse current magnitudes, and the results are compared with the type test data provided by the manufacturer. Fig. B2 shows the result for 5 kA impulse where the voltage across the SVL is limited to 20 kV.

References

[1] IEC 60141-1:1993, Tests on Oil-filled and Gas-pressure Cables and Their Accessories – Part 1: Oil-filled, Paper or Polypropylene Paper Laminate Insulated, Metal-sheathed Cables and Accessories for Alternating Voltages up to and Including 500 kV, 1993.
[2] CIGRE WG C4.502, Power system technical performance issues related to the application of long HVAC cables, CIGRE Tech. Broch. (October (556)) (2013).
[3] F. Ghassemi, Effect of trapped charges on cable SVL failure, in: IPST 2013, Paper ID-219, Vancouver (Canada), June, 2013.
[4] M. Takaoka, The potential distribution of direct current oil-filled cable, IEEE Trans. Power Appar. Syst. PAS-90 (6) (1971) 2622–2630.
[5] I. Lafaia, F. Ghassemi, A. Ametani, J. Mahseredjian, S. Dennis, A. Haddad, S. Robson, Experimental and theoretical analysis of cable discharge, IEEE Trans. PWRD 32 (August (4)) (2017) 2022–2030, http://dx.doi.org/10.1109/TPWRD.2016.2602361.
[6] A. Ametani, C.T. Wan, Sheath overvoltages due to a fault on an EHV cable, IPST-1995 (1995) 87–92.
[7] P. Tant, B. Bolsens, T. Sels, D. Van Dommelen, J. Driesen, R. Belmans, Design and application of a field mill as a high-voltage DC meter, IEEE Trans. Instrum. Meas. 56 (4) (2007).
[8] F. Ghassemi, S. Dennis, A. Ainsley, A. Haddad, S. Robson, Measurement of cable trapped charges and discharge, in: EEUG 2016 Conference, Paper 104, Birmingham, UK, September, 2016.

Table B1
SVL90 V–I characteristic.

I (A)	0.0141	0.0424	0.0707	0.7071	1.4142	2.8284	6.6468	2050.61	4949.75	10182.34	15556.4	43840.6
V (V)	4242.6	12727.9	14142.1	14849.2	15556.3	16263.5	16617	18384.8	19799	21213.2	22344.6	25455.8